2010 IEEE International Conference on Robotics and Automation
Anchorage Convention District
May 3-8, 2010, Anchorage, Alaska, USA

A New Method of Modeling the Actuation Dynamics of a Miniature Hingeless Helicopter Using Gyroscopic Moments

Tak Kit Lau, Yun-hui Liu, *Fellow, IEEE* and Kai-wun Lin

Abstract— **For years, the puzzling cross-coupled responses between the control axes on the hingeless helicopters have long been haunting researchers. Different from previous works that underestimated the gyroscopic moments as a minor off-axis cross-coupling and misinterpreted the precession phenomena on the rotors of the hingeless helicopters as a phase-lag which is physically meaningless, this paper proposes a new method to relate both on-axis and off-axis responses by the influential gyroscopic moments through the actuation mechanism of the hingeless helicopters. Therefore, by this new method the debatable cross-coupling due to actuation dynamics can be directly and analytically quantified. This method is based on the fact that when the angular momentum of the spinning rotor is disturbed by the incremental lift along the main blades due to the varying cyclic pitch angle controlled by the servo mechanisms, the off-axis moments are induced to counteract the changes of the angular momentum according to the principle of gyroscope, and hence these gyroscopic moments directly exhibit the on-axis responses. This new method yields a parametric framework to examine the previously unexplained cross-coupled responses on the hingeless helicopters, and it shows that in hingeless helicopters except the aerodynamics the intricate nonlinearities are also attributed to their unintuitive actuation mechanisms. Finally, simulations as well as experiments have been carried out to validate the proposed modeling method.**

I. Introduction

Unmanned aerial robots have been arousing many attentions from numerous research groups worldwide over the last decade [1]. Among all aerial vehicles, helicopters are often utilized as the platforms to equip with unmanned technology in virtue of its agile ability in hovering and six-degree-of-freedom movement to carry out missions, such as power line inspections [2], pin-pointed hovering [3] and shipboard landing [4], in which fixed-wing vehicles cannot achieve. Moreover, the miniature helicopters, in particular, are capable of performing aggressive aerobatics [5] due to its high power-to-weight ratio, and are inexpensive and conveniently available in the Radio Control (R/C) market. Hence they are becoming more and more popular for experimental flight tests and daily use. Within all kinds of miniature helicopters, one of the subclasses, the hingeless helicopter, is particularly attractive for unmanned aerial vehicle (UAV) development because its uncomplicated rotor design that has feathering but no flapping [6] (See Fig. 1). It yields a more responsive maneuverability to commands.

However, one coin has two sides. The notorious dark side of the mechanically elegant and responsive hingeless helicopters is on the aspect of controlling such a highly nonlinear and coupled dynamics. For years, due to the unclear causes of the cross-coupling on every axis-pair on helicopters, no publication addresses this kind of coupled nonlinearity, such as the sideslip due to pitch effect [7]. Some attempted to predict these auxiliary responses, but none of them is even correct in the prediction of signs when compared against the experimental data [8]. Therefore, in the phase of controller design, these ubiquitous couplings are often not predicted. Instead, they are minimized by mixing the control inputs in a trial-and-error manner according to the pilot experience [9].

Previous work [10][11] on the modeling of the hingeless helicopters from the actuation mechanism to the aerodynamics, without an exception, introduced a phase-lag to the cyclic pitch angle hence the incremental lift along the main blades can be instinctively understood. This study derives a parametric model of the actuation mechanism on the hingeless helicopters in terms of the cyclic pitch angle and inputs to the swashplate. And, based on these analytical forms, this study analyses the dynamics of rotor and fuselage by the principle of gyroscopic phenomena. The main idea of this treatment is that when the angular momentum of the spinning rotor is disturbed by the incremental lift along the main blades due to the varying cyclic pitch angle under different commands, the disturbed angular momentum induces an moment to counteract the disturbance according to the principle of gyroscope. This sequence of actions introduces the cross-couplings to the overall helicopter dynamics. The significance of this work is that, without introducing the previously used magical phase-lag, the proposed method is validated both in simulations and experiments that using the gyroscopic moments this study explain the actuation dynamics of the hingeless helicopters and quantified the coupled dynamical responses that cannot be addressed by the previous analysis. Also, this new treatment enables the design of nonlinear autopilot for the miniature hingeless helicopters to account for the often neglected coupled dynamics, and extends the understanding of dynamics in this kind of aerial vehicles.

II. Input-Output Relation Of Hingeless Helicopters

Hingeless helicopters differ from other miniature helicopters in their rotor design. The rotor is actuated concurrently through three servomechanisms via a swashplate (Fig. 2). The swashplate is designed with an outer ring and an inner ring. The outer ring of the swashplate connects with these three servomechanism with a typical 120^o-spacing swashplate. Some other configurations include three servomechanisms with 180^o-spacing and 140^o-spacing, and four servomechanisms with 90^o-spacing. The analysis of the actuation mechanism that uses different types of swashplate are similar, and this study focuses on the 120^o-spacing type. The inner ring connects the swashplate with the upper part of the rotor via two sets of ball-bar linkages. One set connects

This work was partially sponsored by the Hong Kong RGC under the grants 414406 and 414707. T.K. Lau, Y.H. Liu and K.W. Lin are with the Department of Mechanical and Automation Engineering, The Chinese University of Hong Kong, China. E-mail: {tklau,yhliu,kwlin}@mae.cuhk.edu.hk.

with the rotary joints of the main blades and changes the pitch angle directly, while the other set connects to the shaft of flybar through a three-bar-linkage. This mechanism is shown in Fig. 1.

The purpose of all mechanisms are designed to vary the pitch angles, which is also known as the angles of attack, on the main blades. As the blades spin with the rotor and the inner ring of the swashplate but not the whole swashplate, hence for a certain tilting posture of the swashplate, the pitch angles on the two main blades vary cyclically according to the linkages in which the swashplate manipulates.

Using the geometries shown in Fig. 3, the cyclic pitch angle of the main blades in terms of the direct and indirect input can be derived, such that,

$$\frac{L_{11}\sin\beta + \delta_{cyc} + \delta_{cyc_o}}{L_2 + L_3} = \frac{L_1 \sin\left(\theta_{cyc} + \theta_{cyc_o}\right) + \delta_{cyc} + \delta_{cyc_o}}{L_2} \tag{1}$$

To write the cyclic pitch angle,

$$\theta_{cyc} = \sin^{-1}\left[\left(\frac{L_2\left(L_{11}\sin\beta + \delta_{cyc}\right)}{L_{12}\left(L_2 + L_3\right)} - \frac{\delta_{cyc}}{L_{12}}\right) + \sin\theta_{cyc_o}\right] \tag{2}$$

Where θ_{cyc} is the cyclic pitch angle. δ_{cyc} is the direct input. δ_{cyc_o} and θ_{cyc_o} are the initial displacement and angle at which the throttle command is at initial zero. β is the paddle flapping angle. The direct input can be written as a first order Fourier series, such that,

$$\delta_{cyc}\left(\psi_R\right) = \delta_\phi \cos\psi_R + \delta_\theta \sin\psi_R + \delta_{cyc}^{thro} \tag{3}$$

Where δ_ϕ is the roll displacement input, δ_θ is the pitch displacement input. δ_{cyc}^{thro} is the displacement input due to throttle command, and each servomechanism have the same displacement. For the roll displacement input, only the joint aileron and joint pitch as shown in Fig. 2 are involved. However, for the pitch displacement input, all joints, including the joint elevator are involved.

The flapping angle of the paddles in (2) can be derived using the geometry in Fig. 4, such that,

$$\sin\beta = \frac{\delta_{fly}}{L_6} \tag{4}$$

Where δ_{fly} is the indirect input. It can be derived using geometry as well, such that,

$$\begin{aligned}\delta_{fly} &= \frac{L_5}{L_4}\left(-L_4\sin\theta_{r1_o} + \delta_\theta\right) - \left(-L_5\sin\theta_{r1_o}\right) \\ &= \frac{-L_4L_5\sin\theta_{r1_o} + L_5\delta_\theta + L_4L_5\sin\theta_{r1o}}{L_4} \\ &= \frac{L_5}{L_4}\delta_\theta\end{aligned} \tag{5}$$

As the rotor spins and therefore the inputs from the swashplate to the cyclic pitch angles via the direct and indirect inputs varies according to the azimuth angle, ψ_R. Rewrite (5),

$$\delta_{fly}\left(\psi_R\right) = \frac{L_5\left(\delta_\theta\sin\psi_R + \delta_\phi\cos\psi_R\right)}{L_4} \tag{6}$$

Substituting (3), (4) and (6) into (2), the analytical form that describes the variation of the cyclic pitch angle of a main blade in a revolution is obtained. The results is shown in Fig. 5. From the numerical analysis, the inputs to the cyclic pitch angles can be therefore approximated as a Fourier series,

$$\theta_{cyc}\left(\psi_R\right) = \delta_\phi a_{cyc}\cos\psi_R + \delta_\theta b_{cyc}\sin\psi_R + c_{cyc} \tag{7}$$

Where $a_{cyc}, b_{cyc}, c_{cyc}$ are coefficients according to the instantaneous throttle command. These coefficients can be directly evaluated from calibrations. In this section, the input-output relation between the prime variable, the cyclic pitch angle of the main blade, and the control inputs from servomechanisms are derived. And the result is used in the next section to discuss the influence of this variable in the overall helicopter dynamics through the principle of gyroscopic effect.

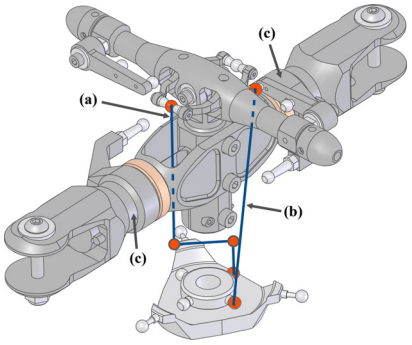

Fig. 1. (a) A three-bar-linkage from the inner ring of the swashplate to the flybar. It rotates the angle of attack of the paddles and hence alters the inclination of the hub plane of paddles. It serves as an indirect input to the cyclic pitch angle of the main blades. (b) A single-linkage that connects the inner ring to the leverage set. It directly alters the cyclic pitch angle, and therefore it serves as a direct input. Regarding to the feathering and flapping, the hingeless rotor is designed to exhibit feathering but no flapping [6]. However, the mild flapping, which can be observed along the main blade axis on the rotor, is due to the elasticity of the rubber shock absorbers inside (c), and it strengthens the incremental lifting moments along the blades. It imposes no effect on the directions of these moments.

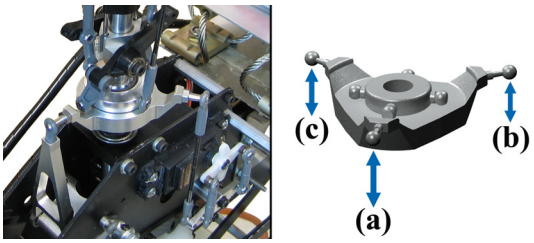

Fig. 2. Left: A 120^o-spacing swashplate of a hingeless helicopter. Right: Each joint on the swashplate connects with a servomechanism which is placed below the plate. A naming convention is employed, such that (a) Joint Elevator, (b) Joint Aileron, (c) Joint Pitch.

III. Helicopter Dynamics

In this section, the manipulation of the helicopter's dynamics due to the cyclic pitch angles is discussed. First, the frames of reference are defined. The body frame of the hingeless helicopter is defined at the hub point O_B. To ease the calculation of inertia tensor of the spinning rotor, a frame is attached on the rotor at O_R, which is at the hub point as well. The inertial coordinate frames, body frame and the rotor coordinate frame are represented with their unit directional

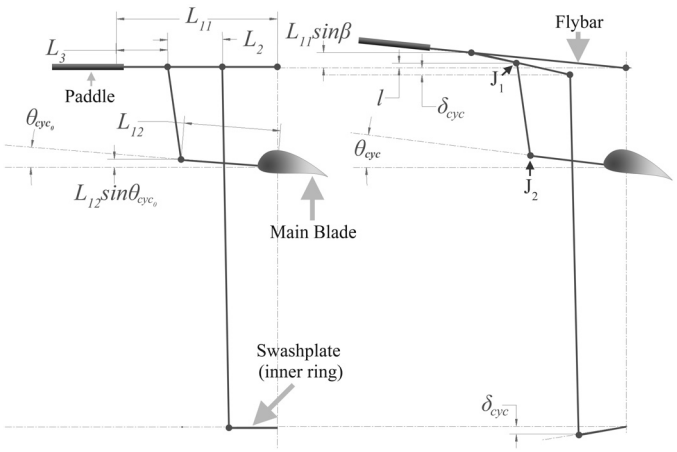

Fig. 3. The side-view of the schematics of the flybar-rotor structure. It describes the movement of linkages when the swashplate tilts for an input δ_{cyc} and the flybar flaps for an angle β.

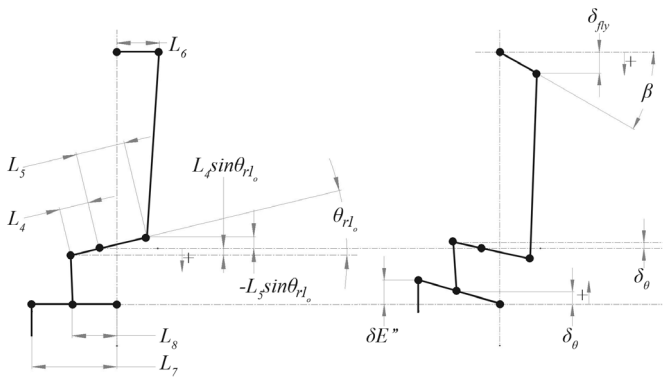

Fig. 4. The schematics of the indirect input. The indirect input directly influences the flapping angle of the flybar, and hence the cyclic pitch angle is eventually altered. $\delta E''$ is the input from the joint elevator.

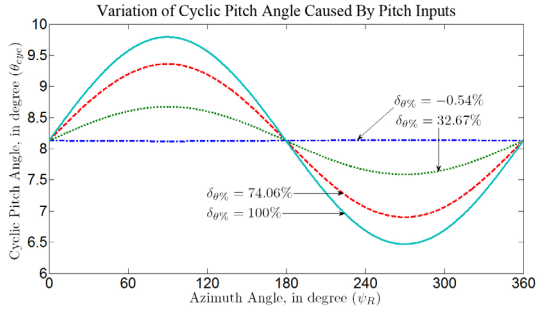

Fig. 5. Using the analytical forms (3), (5) and (2), this figure plots the variation of the cyclic pitch angles of a main blade in a function of azimuth angle. The control commands are recorded from a commercially available manual controller, JR PCM9XII, then goes into the analytical forms to obtain the resultant cyclic pitch angle at an azimuth angle.

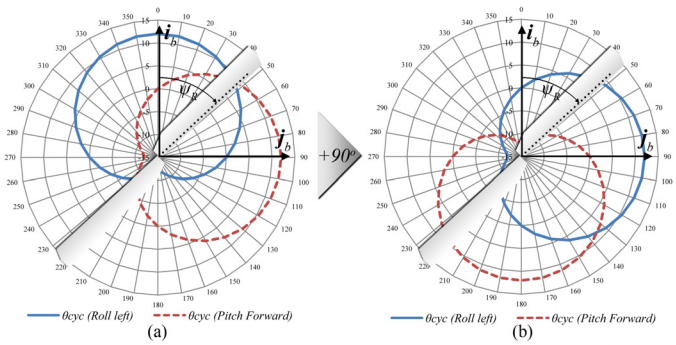

Fig. 6. (a): The actual variation of the cyclic pitch angle on the main blades in a revolution, it can be measured directly from the blades. The rotation angle ψ_R is defined positively around the z-axis of the body frame. This variation cannot be intuitively understood because, for example, to roll left, more lift should be generated on the right hand side of the hub plane, instead of the front side. (b): The compensated variation of the cyclic pitch angle after going through a conventional phase-lag treatment, such that the cyclic pitch angles are added by a 90^o as a phase lag. Except being wrong, it then becomes *intuitively understandable* because, for example, to roll left (blue solid line), more lift are generated on the right side of the hub plane.

vectors,

$$\sum I = \{\mathbf{i}, \mathbf{j}, \mathbf{k}\}$$
$$\sum B = \{\mathbf{i}_B, \mathbf{j}_B, \mathbf{k}_B\}$$
$$\sum R = \{\mathbf{i}_R, \mathbf{j}_R, \mathbf{k}_R\}$$

Using transport theorem [12], the helicopter dynamics is expressed as,

$$\sum \mathbf{F} = m\dot{\mathbf{v}} + m\left(\boldsymbol{\omega} \times \mathbf{v}\right) \tag{8}$$

$$\sum \mathbf{M} = \dot{\mathbf{H}} + \boldsymbol{\omega} \times \mathbf{H} \tag{9}$$

Where $\sum \mathbf{F}$ is the total external forces acting on the fuselage at the hub point, and is expressed in the body frame. $\mathbf{v}$ is the velocity of the fuselage at the hub point with respect to the body frame. $\boldsymbol{\omega}$ is the angular velocity of the fuselage at the hub point with respect to the inertial frame. For the rotational dynamics, $\mathbf{H}$ is the angular momentum of the fuselage. $\boldsymbol{\omega}$ is the angular velocity of the fuselage with respect to the inertial frame.

A. Aerodynamics

The aerodynamics on the helicopter is well studied in previous work [9][13] based on blade element theory [14], so the equations are directly given here. For the thrust,

$$\mathbf{T} = -\left[\frac{n}{12\pi}\rho c a \Omega^2 \left(BR\right)^3 \int_0^{2\pi} \theta_{cyc} d\psi_R\right] \mathbf{k}_B \tag{10}$$

Where n is the number of blades, ρ is the air density, c is the chord length, a is the lift curve slope, B is the tiploss factor, R is the length of a main blade and Ω is the spinning speed of the main rotor, θ_{cyc} is the cyclic pitch angle. ψ_R is the azimuth angle. In (9), the sum of moments can be decomposed of several moments due to lifting, deadweight, motor torque and drag, such that,

$$\sum \mathbf{M} = \mathbf{M}_G + \mathbf{M}_L + \mathbf{M}_t + \mathbf{M}_W + \mathbf{M}_M + \mathbf{M}_D \tag{11}$$

Where all the moments are total external moments acting on the fuselage due to the gyroscopic effect of the spinning rotor ($\mathbf{M}_G$), uneven incremental lift along main blades ($\mathbf{M}_L$), tail rotor thrust ($\mathbf{M}_t$), deadweight ($\mathbf{M}_W$), motor torque ($\mathbf{M}_M$)

and aerodynamic drag ($\mathbf{M}_D$). The aerodynamics drag can be derived as,

$$\mathbf{M}_D = \frac{n}{3}\rho c a \Omega^2 (BR)^3 \mathbf{k}_B \tag{12}$$

The incremental lift along the main blades with respect to the body frame is derived by considering the instantaneous lift through the integration for a revolution, such that,

$$\mathbf{M}_L = \rho c a \Omega^2 (BR)^4 \begin{bmatrix} -\int_0^{2\pi} \theta_{cyc}(\psi_R) \sin\psi_R d\psi_R \mathbf{i}_B \\ \int_0^{2\pi} \theta_{cyc}(\psi_R) \cos\psi_R d\psi_R \mathbf{j}_B \\ 0 \end{bmatrix} \tag{13}$$

Where ψ_R is the azimuth angle which is defined about negative z-axis of the body frame of the helicopter. For the tail thrust and its according moment,

$$\mathbf{T}_t = -\left[\frac{n_t}{6}\rho c_t a_t \Omega_t^2 \theta_{tail} (BR_t)^3\right] \mathbf{j}_B \tag{14}$$

$$\mathbf{M}_t = \mathbf{r}_t^b \times \mathbf{T}_t \tag{15}$$

Where $\mathbf{r}_t^b$ is the position vector of the tail hub point with respect to the body frame, θ_{tail} is the pitch angle of the tail blade, R_t is the radius of the tail blade, c_t is the chord length, a_t is the lift curve slope, and Ω_t is the spinning speed of the tail which can be obtained using gear ratio, and the ratio is 8:1 for JR Voyager GSR. For the deadweight and its moment on the helicopter,

$$\mathbf{W}^b = mg \begin{bmatrix} -\sin\theta \\ \sin\phi\cos\theta \\ \cos\phi\cos\theta \end{bmatrix} \tag{16}$$

$$\mathbf{M}_w^b = \mathbf{r}_{cg}^b \times \mathbf{W}^b \tag{17}$$

Where $\mathbf{W}^b$ is the deadweight acting on the fuselage with respect to the body frame, $\mathbf{r}_{cg}^b$ is the position vector of the center of mass with respect to the body frame, m is the mass of the helicopter, g is the gravity. $[\ \phi \quad \theta \quad \psi\ ]^T$ are attitude angles (Euler angles), namely roll, pitch and yaw. The aerodynamics equations and helicopter dynamics equations are used in section III-C. The precession on the hingeless helicopters is discussed in the next section.

B. Discrepancy and Conventional Treatment

Intuitively, to actuate the hingeless helicopter to pitch forward or backward, and to roll left or right, the cyclic pitch angle should attain larger angles of attack at the side opposite to the direction that of intended. Such that, as shown in Fig. 6 (b), to pitch forward, more lift *should* be generated at the rear side of the hub plane, hence the helicopter can nose down (inclined forward) and translate into the forward movement.

However, the actual variation of the cyclic pitch angle is not coherent with the intuitive expectation. From the actuation mechanism of hingeless helicopters, in Section II the cyclic pitch angle in terms of the control inputs is derived. Using (7), the variation of the cyclic pitch angle is plotted and shown in Fig. 6. It is found that the actual variation of the angle of attack for a revolution is different from the intuitive understanding that this angle should behave in response to pitching or rolling commands.

Previous work [10][15][16] account for this discrepancy by introducing a 90^o phase lag in the name of precession. It is, thus, the cyclic pitch angle varies in an intuitive manner after adding a 90^o as a compensation, such that Fig. 6 (a) becomes (b) after applying the conventional compensation. But the precession is not as magical as adding 90^o to the cyclic pitch angle. The discussion on this claim is furthered in the next section.

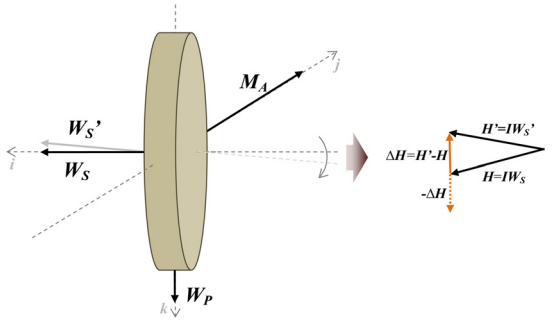

Fig. 7. When a moment ($\mathbf{M_A}$) is applied on an axis perpendicular to the spinning axis of an object, the moment will change the direction of the object as well as the spinning direction. Therefore, by conservation, the change of angular momentum ($\Delta\mathbf{H} = \mathbf{H}' - \mathbf{H}$) will induce an opposite counterpart ($-\Delta\mathbf{H}$), and this angular momentum has a spinning velocity $\mathbf{W_P}$, which is also known as the velocity of precession.

C. Gyroscopically Induced Moment

Different from previous work that introduced a physically meaningless 90^o phase-lag to the cyclic pitch angle and underrated the influence of gyroscopic moments, our proposed treatment, on the contrary, analyzes the overall dynamics of the spinning rotor and the fuselage by considering the gyroscopic moments which is induced by the unintuitive variation of the cyclic pitch angle. Precession [12], or gyroscopic precession, is a phenomena for all spinning bodies that when a spinning body is disturbed, such that its angular momentum is altered, then a moment will be induced on the axis perpendicular to the axis of spinning and the axis of the applied disturbing moment. For example, in Fig. 7, the spinning disc has an angular momentum $\mathbf{H}$ about axis $\mathbf{i}$. When a disturbing moment $\mathbf{M}_A$ is applied on axis $\mathbf{j}$, the altered angular momentum $\mathbf{H}'$ forms the rate of change of angular momentum $\Delta\mathbf{H}$. By the conservation of angular momentum, a moment $\mathbf{M}_P$ is induced to counteract the changes on the angular momentum, such that,

$$\lim_{\Delta t\to 0} -\frac{\Delta\mathbf{H}}{\Delta t} = \lim_{\Delta t\to 0} -\left(\frac{\mathbf{H}' - \mathbf{H}}{\Delta t}\right) = \mathbf{M}_P \tag{18}$$

The induced moment precesses the spinning disc about the axis of precession $\mathbf{k}$. The rate of precession is $\mathbf{W}_P$.

Considering the spinning rotor as a subsystem, to model the induced moment on the spinning rotor due to the gyroscopic effect, first its rate of change of the angular momentum is expressed by transport theorem [12],

$$\mathbf{M}_R = \dot{\mathbf{H}}_R + \boldsymbol{\omega}_R \times \mathbf{H}_R \tag{19}$$

Where $\mathbf{M}_R$ is the total moments acting on the rotor with respect to inertial frame and is expressed in the moving frame, which is attached on the rotor. $\mathbf{H}_R$ is the angular momentum of the rotor, $\boldsymbol{\omega}_R$ is the angular velocity of the rotor with respect to inertial frame. The purpose of attaching the moving frame on the rotor is to ease the calculation of the moment of inertia tensor, such that the tensor can be constant to the moving frame. To express the angular velocity of the rotor,

$$\begin{aligned} \boldsymbol{\omega}_R &= \dot{\psi}_R \mathbf{k} + \dot{\psi}\mathbf{K} + \dot{\theta}\mathbf{J}_1 + \dot{\phi}\mathbf{I}_2 \\ &= \begin{bmatrix} \dot{\psi}\left(-C_{\psi_R}S_\theta + S_{\psi_R}S_\phi C_\theta\right) + \dot{\theta}S_{\psi_R}C_\phi + \dot{\phi}C_{\psi_R} \\ \dot{\psi}\left(S_{\psi_R}S_\theta + C_{\psi_R}S_\phi C_\theta\right) + \dot{\theta}C_{\psi_R}C_\phi - \dot{\phi}S_{\psi_R} \\ \dot{\psi}_R + \dot{\psi}C_\phi C_\theta - \dot{\theta}S_\phi \end{bmatrix} \end{aligned} \tag{20}$$

Where $\dot{\psi}_R$ is the rate of azimuth angle. $[\ \dot{\phi} \quad \dot{\theta} \quad \dot{\psi}\ ]^T$ are the rate of Euler angles, namely roll, pitch and yaw. $\mathbf{k}$ is

the z-axis of the moving frame attached on the rotor, $\mathbf{J}_1$ is the y-axis after rotation about z-axis of the inertial frame by yaw, $\mathbf{I}_2$ is the x-axis after rotation about y-axis of the first transition frame by pitch. The abbreviations for cos and sin are employed, such that $\sin\theta = S_\theta$.

By substituting (20) into (19) to have (21), the gyroscopically induced moment acting on the rotor,

$$\mathbf{M}_R = \begin{bmatrix} {}^R I_x \begin{bmatrix} \ddot{\psi}\left(-C_{\psi_R}S_\theta + S_{\psi_R}S_\phi C_\theta\right) + \dot{\psi}\left(\dot{\psi}_R S_{\psi_R}S_\theta - \dot{\theta}C_{\psi_R}C_\theta + \dot{\psi}_R C_{\psi_R}S_\phi C_\theta + \dot{\phi}S_{\psi_R}C_\phi C_\theta - \dot{\theta}S_{\psi_R}S_\phi S_\theta\right) + \\ \ddot{\theta}S_{\psi_R}C_\phi + \dot{\theta}\dot{\psi}_R C_{\psi_R}C_\phi - \dot{\theta}\dot{\phi}S_{\psi_R}S_\phi + \ddot{\phi}C_{\psi_R} - \dot{\phi}\dot{\psi}_R S_{\psi_R} \end{bmatrix} \\ {}^R I_y \begin{bmatrix} \ddot{\psi}\left(S_{\psi_R}S_\theta + C_{\psi_R}S_\phi C_\theta\right) + \dot{\psi}\left(\dot{\psi}_R C_{\psi_R}S_\theta + \dot{\theta}S_{\psi_R}C_\theta - \dot{\psi}_R S_{\psi_R}S_\phi C_\theta + \dot{\phi}C_{\psi_R}C_\phi C_\theta - \dot{\theta}C_{\psi_R}S_\phi S_\theta\right) + \\ \ddot{\theta}C_{\psi_R}C_\phi - \dot{\theta}\dot{\psi}_R S_{\psi_R}C_\phi - \dot{\theta}\dot{\phi}C_{\psi_R}S_\phi - \ddot{\phi}S_{\psi_R} - \dot{\phi}\dot{\psi}_R C_{\psi_R} \end{bmatrix} \\ {}^R I_z\left(\ddot{\psi}_R + \ddot{\psi}C_\phi C_\theta - \dot{\psi}\dot{\phi}S_\phi C_\theta - \dot{\psi}\dot{\theta}C_\phi S_\theta - \ddot{\theta}S_\phi - \dot{\theta}\dot{\phi}C_\phi\right) \end{bmatrix} \\ + \begin{bmatrix} \left[\dot{\psi}\left(S_{\psi_R}S_\theta + C_{\psi_R}S_\phi C_\theta\right) + \dot{\theta}C_{\psi_R}C_\phi - \dot{\phi}S_{\psi_R}\right]\left(\dot{\psi}_R + \dot{\psi}C_\phi C_\theta - \dot{\theta}S_\phi\right)\left({}^B I_z - I_y^R\right) \\ \left[\dot{\psi}\left(-C_{\psi_R}S_\theta + S_{\psi_R}S_\phi C_\theta\right) + \dot{\theta}S_{\psi_R}C_\phi + \dot{\phi}C_{\psi_R}\right]\left(\dot{\psi}_R + \dot{\psi}C_\phi C_\theta - \dot{\theta}S_\phi\right)\left(-{}^B I_z\right) \\ \left[\dot{\psi}\left(-C_{\psi_R}S_\theta + S_{\psi_R}S_\phi C_\theta\right) + \dot{\theta}S_{\psi_R}C_\phi + \dot{\phi}C_{\psi_R}\right]\left[\dot{\psi}\left(S_{\psi_R}S_\theta + C_{\psi_R}S_\phi C_\theta\right) + \dot{\theta}C_{\psi_R}C_\phi - \dot{\phi}S_{\psi_R}\right]\left(I_y^R\right) \end{bmatrix} \end{bmatrix} \tag{21}$$

The $diag\left(I_x^R, I_y^R, I_z^R\right)$ is the inertia tensor of the rotor. As the spinning rotor is subjected to a change of angular momentum due to the disturbing moments, primarily is the lifting moment, by the conservation of angular momentum, a moment is gyroscopically induced to counteract the change. This induced moment acts on the rotor, as well as on the fuselage. By a transformation using the azimuth angle, this gyroscopically induced moment which acts on the fuselage is,

$$\mathbf{M}_G = -\begin{bmatrix} C_{\psi_R} & S_{\psi_R} & 0 \\ -S_{\psi_R} & C_{\psi_R} & 0 \\ 0 & 0 & 1 \end{bmatrix}\mathbf{M}_R \tag{22}$$

Where $\mathbf{M}_G$ is the induced moment acting on the fuselage by the rotor in (11). The negative sign indicates that the induced rate of change of the angular momentum is an opposite counterpart to the rate of change of the angular momentum due to the external disturbing moments.

IV. Validation

The purpose of this study is to model the hingeless helicopters without using the phase lag as in the previous work. In section III-C, the gyroscopically induced moment is derived and therefore, in this section, the proposed analytical forms via a numerical approach is analysed to observe, for example, whether the helicopter pitches forward, such that it rotates negatively about y-axis of the body frame, when more lift are generated by the main blades to rotate the helicopter negatively about the x-axis of the body frame. Considering the fact that in previous work the prediction of the cross-coupling is not even correct in signs [8], therefore it is crucial (1) to verify whether the proposed treatment can predict the on-axis responses when the hingeless helicopter is commanded to pitch and roll; (2) to obtain the sign of the coupled off-axis responses in order to compare them against the experimental data. It is found that the proposed treatment not only yields the intuitive responses without introducing the conventional 90^o compensation, but it also quantifies the coupled auxiliary responses that previous analysis cannot address.

A. Numerical Simulation

Using MATLAB Simulink the system is numerically modeled using (9), (13), (17) and (22), the overall responses of the hingeless helicopter due to the commands to pitch forward and backward are obtained and shown in Fig. 8. The moment of inertia of the spinning rotor are determined using the SolidWorks with detailed measurements of dimensions and weights. In this simulation, the helicopter is commanded to pitch forward then backward, hence the response should

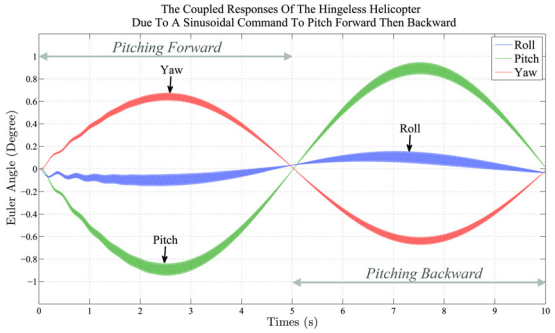

Fig. 8. The responses on the attitude angles of a hingeless helicopter using the proposed treatment. The helicopter is commanded to pitch forward then backward sinusoidally. The responses in the pitch channel is coherent with the commands that it correctly exhibits a motion of pitching forward then a backward motion. Also, it demonstrates the off-axis responses on the roll and yaw channels. Extensive simulations are performed on other axis-pairs, and the on-axis and off-axis relations are summarized in Table. I. The off-axis responses in the yaw channel are described, however, as that results can open another discussion on the tail hunting which is often attributed to the change of motor torque and insufficient of feedback from the autogyro, this aspect is not further discussed in this paper. For the discrepancy in the magnitudes when comparing with the experimental results in Fig. 10, it is accounted to the experiment setup which took place on ground, and the elasticity of the rubber shock absorber (Fig. 1) which strengthens the incremental lifting moments to a yet determined degree of magnitude.

intuitively on the y-axis of the body frame only, namely the pitch channel, and it is the expected result by using the conventional 90^o phase compensation analysis. However, by using our proposed treatment which takes gyroscopic moments into account, it is found that using the proposed analysis that takes the spinning rotor into consideration, except the intuitive on-axis response on the pitch channel, there are coupled off-axis responses in roll and pitch channels when the hingeless helicopter is commanded to pitch forward and backward. Apart from pitching commands, similar responses are obtained when the helicopter is subjected to the rolling commands. The signs of these cross-coupling can be summarized in Table I. This table is empirically validated in the next section IV-B.

B. Experimental Verification

From the numerical simulation of the proposed actuation dynamics of hingeless helicopters, a set of auxiliary responses are revealed in every axis-pair. Therefore, as a validation of the proposed treatment, the fully instrumented hingeless helicopter, JR Voyager GSR, is utilized to record the attitude responses due to different actuation commands by using the onboard computer and Xsens MTi IMU which samples at 100Hz. The experiments are carried out on ground

TABLE I

SUMMARY OF THE CROSS-COUPLING OFF-AXIS RESPONSES

	Pitch Forward	**Pitch Backward**
Primary Axis	y-axis (−)	y-axis (+)
Auxiliary Axis	x-axis (−)	x-axis (+)
	Roll Left	**Roll Right**
Primary Axis	x-axis (−)	x-axis (+)
Auxiliary Axis	y-axis (+)	y-axis (−)
Remarks: All are in body axes.		

Fig. 9. In the experiments, the fully instrumented hingeless helicopter (JR Voyager GSR) is commanded to pitch and roll on the ground. The onboard computer records the inputs to the rotor from servomechanisms, and the IMU measures the inclination information.

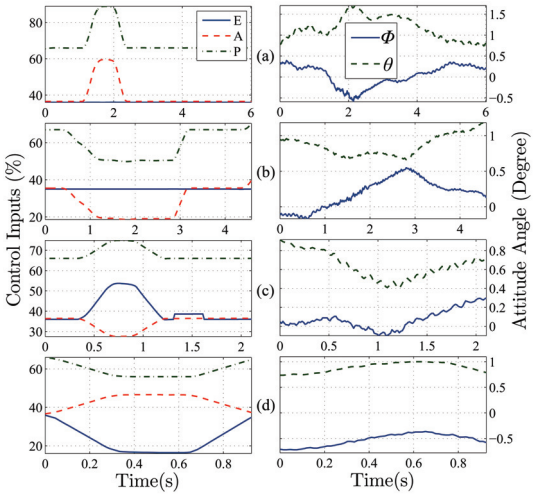

Fig. 10. These figures plot the responses in the attitude angles due to different pitching and rolling commands. (a) *Rolling left command*: the coupled auxiliary response take place positively in the pitch channel; (b) *Rolling right command*: the coupled auxiliary response take place negatively in the pitch channel; (c) *Pitching forward command*: the coupled auxiliary response take place negatively in the roll channel; (d) *Pitching backward command*: the coupled auxiliary response take place positively in the roll channel. These results demonstrate that the predicted auxiliary responses unintuitively exist and influence the overall dynamics. More, the signs of both on- and off-axis responses are coherent with the predictions.

instead of on air because it can rule out the disturbance due to the unmodeled wind gust, and hence the responses can be conclusively distinguished. During the experiments, the rotor is spinning at around 700 to 1,000 revolution per minute, and it is found that that when the helicopter is commanded to pitch forward, the responses takes place not only on the pitch channel, but also on roll channel. More, the signs of the off-axis responses are coherent with the prediction shown in Table. I. In addition, under other pitching and rolling commands, the helicopter also yields the coupled auxiliary responses as predicted (Fig. 10).

V. CONCLUSION

The hingeless helicopters are becoming the popular research platforms in UAV developments worldwide. Researches that utilize the hingeless helicopters are often related to the modeling of their actuation mechanisms and dynamics. This study points out the inadequacy of the previous methods that misinterpreted the precession as simple as a phase-lag when deriving the dynamics model for the hingeless helicopters. Furthermore, this treatment exhibits a comprehensive analysis on the actuation dynamics of the hingeless helicopters by using the gyroscopic effect which takes the influential spinning rotor into the derivation of the overall dynamics. This new treatment not only explains the responses in which the hingeless helicopters intuitively behave, it also quantifies a set of coupled auxiliary responses that the previous work cannot address. To facilitate the verification, this study extensively simulated the derived analytical forms and further, validated them in experiments using the fully instrumented hingeless helicopter. It is found that, using the proposed treatment, the unintuitive off-axis responses can be predicted and the on-axis responses can also be quantified. The significances of this study are that, it analytically extends the understanding of the unclear off-axis responses that the hingeless-type rotorcrafts exhibit in various unmanned applications over the years. Also, it lays a foundation for the vibration analysis, flight quality handling as well as the design of nonlinear flight controller on the hingeless helicopters to fully account for the cross-coupled actuation dynamics which are critical to the precision-guided missions. To author's best knowledge, this is the first paper to correctly relate both on-axis and off-axis cross-couplings due to the actuation dynamics on hingeless helicopters by using the in fact influential but often underestimated gyroscopic moments.

VI. ACKNOWLEDGMENTS

The first author would like to thank the anonymous editor and reviewers for comments.

REFERENCES

[1] K. Valavanis, P. Oh, and L. Piegl, *Unmanned Aircraft Systems: International Symposium on Unmanned Aerial Vehicles, UAV'08*. Springer Verlag, 2008.
[2] L. Mejias, J. Correa, I. Mondragon, and P. Campoy, "COLIBRI: A vision-guided UAV for surveillance and visual inspection," in *2007 IEEE International Conference on Robotics and Automation*, 2007, pp. 2760–2761.
[3] M. Gordon, S. Kondor, E. Corban, and D. Schrage, "Rotorcraft aerial robot-challenges and solutions," in *Digital Avionics Systems Conference, 1993. 12th DASC., AIAA/IEEE*, 1993, pp. 298–305.
[4] M. Negrin, A. Grunwald, and A. Rosen, "Superimposed perspective visual cues for helicopter hovering above a moving ship deck," *Journal of guidance, control, and dynamics*, vol. 14, no. 3, pp. 652–660, 1991.
[5] P. Abbeel, A. Coates, M. Quigley, and A. Ng, "An application of reinforcement learning to aerobatic helicopter flight," in *Advances in Neural Information Processing Systems 19: Proceedings of the 2006 Conference*. The MIT Press, 2007.
[6] Federal Aviation Administration, *Rotorcraft Flying Handbook*. New York: Skyhorse Publishing, 2007.
[7] G. Padfield, *Helicopter flight dynamics: the theory and application of flying qualities and simulation modelling*. Wiley-Blackwell, 2007.
[8] M. Tischler, *Advances in Aircraft Flight Control*. CRC Press, 1996.
[9] J. Leishman, *Principles of Helicopter Aerodynamics*. Cambridge University Press, 2006.
[10] S. Kim and D. Tilbury, "Mathematical modeling and experimental identification of an unmanned helicopter robot with flybar dynamics," *Journal of Robotic Systems*, vol. 21, no. 3, 2004.
[11] B. Mettler, *Identification modeling and characteristics of miniature rotorcraft*. Springer, 2003.
[12] F. Beer, E. Eisenberg, W. Clausen, and G. Staab, *Vector mechanics for engineers, statics and dynamics*. McGraw-Hill Science/Engineering/Math, 2003.
[13] W. Johnson, *Helicopter Theory*. Dover publications, 1994.
[14] W. Stepniewski and C. Keys, *Rotary-wing Aerodynamics*. Dover Publications, 1984.
[15] Federal Aviation Administration, *Pilot's Encyclopedia of Aeronautical Knowledge*. Skyhorse Publishing, Inc., 2007.
[16] J. Welch, L. Bjork, and L. Bjork, *Van Sickle's Modern Airmanship*. McGraw-Hill Professional, 1999.